

Structural determination of the Bi(110) semimetal surface by LEED analysis and *ab initio* calculations

J. Sun,^{1,*} A. Mikkelsen,^{2,†} M. Fuglsang Jensen,² Y. M. Koroteev,^{3,4} G. Bihlmayer,⁵ E. V. Chulkov,^{3,6} D. L. Adams,⁷ Ph. Hofmann,² and K. Pohl¹

¹*Department of Physics and Materials Science Program, University of New Hampshire, Durham, New Hampshire 03824, USA*

²*Institute for Storage Ring Facilities and Interdisciplinary Nanoscience Center (iNano), University of Aarhus, 8000 Aarhus C, Denmark*

³*Donostia International Physics Center (DIPC), 20018 San Sebastián, Basque Country, Spain*

⁴*Institute of Strength Physics and Materials Science, Russian Academy of Sciences, 634021, Tomsk, Russia*

⁵*Institut für Festkörperforschung, Forschungszentrum Jülich, D-52425 Jülich, Germany*

⁶*Departamento de Física de Materiales and Centro Mixto CSIC-UPV/EHU, Facultad de Ciencias Químicas, UPV/EHU, Apartado 1072, 20080 San Sebastián, Basque Country, Spain*

⁷*Institute for Physics and Astronomy, University of Aarhus, 8000 Aarhus C, Denmark*

(Received 16 June 2006; revised manuscript received 5 October 2006; published 6 December 2006)

The surface structure of Bi(110) has been investigated by low-energy electron diffraction intensity analysis and by first-principles calculations. Diffraction patterns at a sample temperature of 110 K and normal incidence reveal a bulk truncated (1×1) surface without indication of any structural reconstruction despite the presence of dangling bonds on the surface layer. Good agreement is obtained between the calculated and measured diffraction intensities for this surface containing only one mirror-plane symmetry element and a buckled bilayer structure. No significant interlayer spacing relaxations are found. The Debye temperature for the surface layer is found to be lower than in the bulk, which is indicative of larger atomic vibrational amplitudes at the surface. Meanwhile, the second layer shows a Debye temperature close to the bulk value. The experimental results for the relaxations agree well with those of our first-principles calculation.

DOI: [10.1103/PhysRevB.74.245406](https://doi.org/10.1103/PhysRevB.74.245406)

PACS number(s): 68.35.Bs, 61.14.Hg

I. INTRODUCTION

Characteristic of group-V elements, bismuth crystallizes in the rhombohedral $A7$ structure as a semimetal with a small density of states at the Fermi level.¹ But interestingly, the surfaces of Bi show very different electronic properties from the bulk. Studies on the Bi(110),² Bi(100),³ and Bi(111) (Refs. 4 and 5) surfaces have shown that they are much more metallic than the bulk due to a significantly higher density of states at the Fermi level at the surface.⁶ It has been found that one significant contribution is from a strong spin-orbit coupling at the surface due to broken inversion symmetry.^{2,6–8}

From a chemical point of view, the creation of a surface requires the breaking of atomic bonds. Covalent bonding plays only a minor role in most metals. Thus the effect of bond breaking is small and surface properties are similar to those of the bulk, although localized electronic surface states may be present. On semiconductors, creating a surface leaves so-called dangling bonds which should give rise to half-filled and therefore metallic bands. However, it turns out that on most semiconductor surfaces the atoms rearrange their positions such that the dangling bonds are removed and the surface is again a semiconductor and not a metal.⁹ Semimetals such as bismuth lie in between these two cases. On one hand, a semimetal is close to being a semiconductor since directional bonding is important and the valence and conduction bands are almost separated by a gap. On the other hand, there is a very small overlap between both bands such that the material is formally a metal. This delicate balance between being a metal and a semiconductor depends crucially on the atomic structure¹⁰ and it can be expected to be severely disturbed at the surface.

Detailed structural information on Bi surfaces is so far limited to a recent low-energy electron diffraction (LEED) intensity vs voltage (IV) and first-principles study of the Bi(111) surface.¹¹ One important difference between bulk-terminated Bi(110) and Bi(111) is that the Bi(110) surface exhibits dangling bonds, while Bi(111) does not. In a pioneering study by Jona,¹² oxygen adsorption experiments suggest that Bi(110) is noticeably more active than Bi(111). A qualitative analysis of LEED patterns in Jona's study shows an unreconstructed (1×1) Bi(110) surface structure. From the bulk structure Jona erroneously concluded that the unit cell (and hence the LEED pattern) should not be exactly rectangular but that the lattice vectors should include an angle slightly different from 90° . This is not correct, as will become apparent below. The unit cell is rectangular and almost square. A recent scanning tunneling microscopy study by Pascual *et al.*,⁸ revealed images of the Bi(110) surface that are consistent with a near-square surface unit cell.

In contrast to most metal surfaces, Bi(110) has a very low symmetry—the only symmetry element being a mirror plane while it has no translational symmetry normal to the surface. This makes the LEED IV analysis of this surface challenging. Along the $[110]$ direction the Bi has a close stacking of atomic layers, i.e., the buckled bilayer as described below that requires the combined space method¹³ to calculate diffraction matrices. The stacked layers have a registry that does not repeat itself, or in other words, the stacking sequence has an infinite repeat distance due to its nonsymmetrical translation parallel to the mirror plane. More importantly, the dangling bonds at the surface may complicate the surface electronic and geometrical structures, which makes this open surface quite similar to many semiconductors and binary compounds.

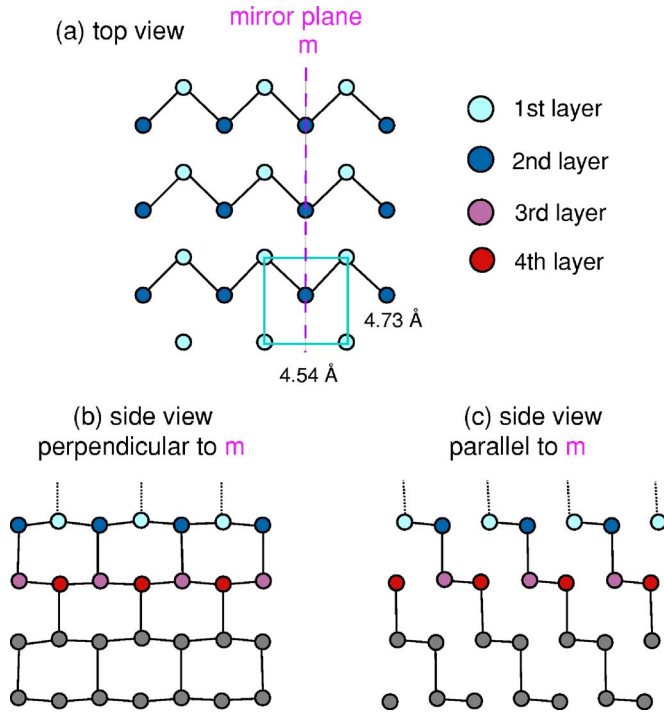


FIG. 1. (Color online) Truncated bulk structure of Bi(110). The solid and dotted lines mark covalent and dangling bonds, respectively. (a) Top view of the first two atomic layers. Each layer consists of a two-dimensional rectangular lattice and the lattice constants at 110 K are given. The mirror planes of the structure are also shown as dashed lines. (b) and (c) Side views of the first eight layers perpendicular and parallel to the mirror plane, respectively. The bilayerlike structure with alternating short and long interlayer spacings is evident.

In this paper, we report on a study of the surface structure of clean Bi(110) by quantitative LEED intensity vs voltage analysis and *ab initio* calculations. Experimental diffraction intensities taken at a sample temperature of 110 K under normal incidence have been analyzed by comparison to dynamical LEED calculations. Great care was taken to align the sample considering the low-symmetry diffraction pattern. The main structural parameters that were optimized in the LEED IV analysis include the first four interlayer spacings and the Debye temperatures for the first two surface layers. Furthermore, we have performed first-principles calculations for the atomic structure of Bi(110). The results are in good agreement with the experimental relaxations.

In the following section, we introduce the bulk truncated surface structure of Bi(110). Experimental and computational details are described in Sec. III, followed by the results and discussion in Sec. IV. Conclusions are given in Sec. V.

II. BULK TRUNCATED Bi(110) SURFACE STRUCTURE

The A7 (α -arsenic) structure of bulk bismuth has a rhombohedral unit cell with a two-atom basis. This structure can be obtained by a slight stretching of two penetrating face-centered cubic structures along the body diagonal.¹⁴ The bulk truncated surface structure of Bi(110) is shown in Fig. 1.

Each atom has three nearest neighbors to which it is connected by quasicovalent bonds. The side views show the stacked bilayers loosely bound by a single bond between every other atom in neighboring bilayers. Within one bilayer, each atom in one layer closely bonds with two nearest-neighbor atoms in the other layer, forming a buckled structure. The covalent bonds have been drawn by solid lines and the dangling bonds at the surface layer by dashed lines. The bilayer-type structure gives rise to alternating interlayer distances. For the truncated bulk at 110 K we have $d_{12}^b = 0.208$ Å, $d_{23}^b = 3.064$ Å, $d_{34}^b = 0.208$ Å, $d_{45}^b = 3.064$ Å, and so on. Interlayer spacings between the i th and j th bulk layers are indicated as d_{ij}^b . Noticeably, the Bi(110) surface has very low symmetry: the only symmetry element is a mirror plane as indicated in Fig. 1. The lengths of unit vectors at 110 K are taken as 4.731 and 4.538 Å; see Refs. 12, 14, and 15. If the rhombohedral structure is treated as a pseudocubic structure as in Ref. 12, Bi(110) will be denoted as Bi(100). The pseudosquare character of the surface unit cell is evident: for a cubic Bi structure all the atoms in the first bilayer would have the same height, the unit cell would be rotated by about 45°, and contains only one atom.

III. METHODS

A. Experiment

The experiment was performed in a μ -metal ultrahigh-vacuum chamber equipped with a four-grid LEED optic with a base pressure of 7×10^{-9} Pa. Surface contamination was measured by Auger electron spectroscopy (AES) using a hemispherical electron analyzer and the LEED electron gun as electron source. The sample was mounted on a manipulator, allowing positioning to within 0.1° around all three axes of the crystal. The sample was cooled by liquid nitrogen. The surface was cleaned by cycles of 1 keV Ar^+ sputtering and annealing to 150 °C. With AES no surface contamination could be detected. The maximum possible oxygen contamination was determined to be 0.02 monolayers. Spot intensities were measured using a 16-bit charge-coupled device (CCD) camera. A back-illuminated and Peltier-cooled (-40 °C) CCD chip guaranteed a high quantum efficiency and low dark current. The camera was mounted on a base that allowed rotation around all three axes. Great care was taken to align the camera with respect to the electron gun and the Bi crystal, as described below.

To obtain intensities of the diffracted beams as a function of electron energy, the following procedure was employed. A series of images was recorded within the energy range from 30 to 300 eV, while the energy was increased in steps of 1 eV after every recorded image. The integrated spot intensity of every single diffracted beam (h, k) was extracted from these images. The presence of only one mirror line symmetry for Bi(110) leads to technical challenges for the LEED experiment. These difficulties are illustrated in Fig. 2 that shows two measured LEED patterns taken at different incident energies. The pseudosquare pattern of the reciprocal lattice and the missing left (right) symmetry are clearly evident. The up (down) symmetry is given by the mirror plane in the crystal (the horizontal plane in Fig. 2). It is necessary to align

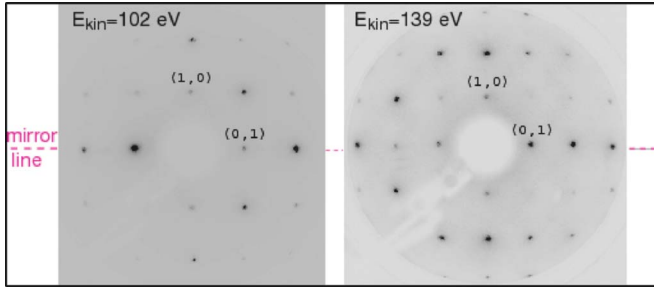


FIG. 2. (Color online) LEED patterns at two different electron beam energies for normal incidence on Bi(110) at 110 K. The (1,0) and (0,1) diffraction spots are marked.

the sample surface perpendicular to the incoming electron beam, and this is usually done by comparing the IV curves of the symmetry-equivalent beams. Here this procedure can only be applied for the up (down) angle. In order to align the left (right) angle we optimized the diffraction spot position on the LEED screen until they agreed with the kinematically calculated positions. We estimate that this approach leads to an error of less than 1° in the angle of incidence. In the final data set, the intensities of the symmetry-equivalent beams were averaged.

B. Dynamical LEED calculations

The dynamical LEED intensity calculations were performed using the standard package SATLEED (symmetrized automated tensor LEED) by Barbieri and Van Hove¹⁶ within the renormalized forward-scattering perturbation formalism. Atomic scattering phase shifts have been calculated using a muffin-tin potential model and the standard Barbieri and Van Hove phase shift package.¹⁶ The bulk diffraction matrices for the closely spaced bilayers were calculated with the combined space method.¹³ The same muffin-tin radius of 2.87 a.u. and phase shifts have been used as in Ref. 11. Phase shifts have been renormalized by the thermal effects of root-mean-square (rms) isotropic vibrational amplitudes. Up to 15 ($L=14$) phase shifts have been used because of the strong scattering of the heavy Bi atom ($Z=83$). The muffin-tin constant V_0 is taken to be energy independent and is optimized. V_{im} , the imaginary part of the inner potential, also referred to as the damping or optical potential, is taken as 4 eV for the bulk and 4.2 eV for the first two overlayers. The slightly larger value at the surface was chosen to model the presence of dangling bonds, which increases the electron damping. The surface potential step of height V_0 is located half a long bulk interlayer spacing away from the topmost layer nuclei. The bulk Debye temperature is fixed at 119 K,¹⁷ while the Debye temperatures for the first two layers are optimized. Mean-square atomic vibrational amplitudes $\langle u^2 \rangle_T$ at temperature T for the Debye-Waller factor calculation are derived from Debye temperatures Θ_D according to the following equation:¹⁸

$$\langle u^2 \rangle_T = \frac{9\hbar^2}{m_a k_B \Theta_D} \left(\frac{T^2}{\Theta_D^2} \int_0^{\Theta_D/T} \frac{x dx}{e^x - 1} + \frac{1}{4} \right), \quad (1)$$

where m_a is the atomic mass, \hbar Planck's constant, and k_B the Boltzmann constant.

In the LEED intensity analysis, agreement between experimental and calculated LEED intensities is quantified by the widely used Pendry R factor R_P , which is particularly sensitive to relative peak position and the existence of small peaks.¹⁹ The uncertainties in the optimized structural parameters are estimated from the variation around the minimum $R_{P \min}$,

$$\Delta R_P = R_{P \min} \times \sqrt{8|V_{im}|/\Delta E}, \quad (2)$$

where ΔE is the total energy range compared in the IV analysis.¹⁹

C. *Ab initio* calculations

We have also performed *ab initio* calculations of the surface crystal structure of Bi(110). The full-potential linearized augmented plane wave method in film geometry^{20,21} as implemented in the FLEUR code was used and the local density approximation²² to the density functional theory was employed. Spin-orbit coupling was included in the self-consistent calculations.²³ The evaluation of the surface relaxation has been carried out for the symmetric 14-layer film, both with the inclusion of the spin-orbit coupling (SOC) term and without this term. Force calculations have been performed for the first four layers without spin-orbit coupling while relaxations have been carried out only for the first two interlayer spacings with the inclusion of SOC. In the latter evaluations we kept the interlayer spacings d_{34} and d_{45} equal to those obtained from the force calculation without SOC. The geometry was chosen such that both sides of the film were terminated with an intact bilayer. A wave-function cutoff of 3.8 a.u.⁻¹ was chosen and the Brillouin zone was sampled with 32 \mathbf{k} points.

IV. RESULTS AND DISCUSSIONS

A. LEED structure determination

The LEED pattern of Bi(110) has previously been discussed by Jona.¹² He defined a pseudocubic bulk unit cell and concluded that the unit cell (and hence the LEED pattern) should not be exactly rectangular but that the lattice vectors should include an angle slightly different from 90° . Our study does not confirm this conclusion. Our LEED patterns as presented in Fig. 2 show an exact rectangular net from careful measurements of the diffraction spots positions and, indeed, such an exact rectangle can also be expected from a projection of the bulk reciprocal lattice onto the surface.⁶ The measured ratio of the two reciprocal unit cell vectors is 0.96(2) in good agreement with the expected value of 0.959. Moreover, the observed patterns show no indication of any reconstruction of the Bi(110) surface, despite the existence of active dangling bond at the surface. Apparently, Bi(110) is found to be very different from typical semiconductor surfaces, such as Si(100) and Ge(100) which both exhibit 2×1 reconstructions.

The structural and nonstructural parameters were optimized for a Bi(110) surface terminated by an intact bilayer. A termination with a split bilayer was immediately excluded due to lack of agreement with the experimental IV curves

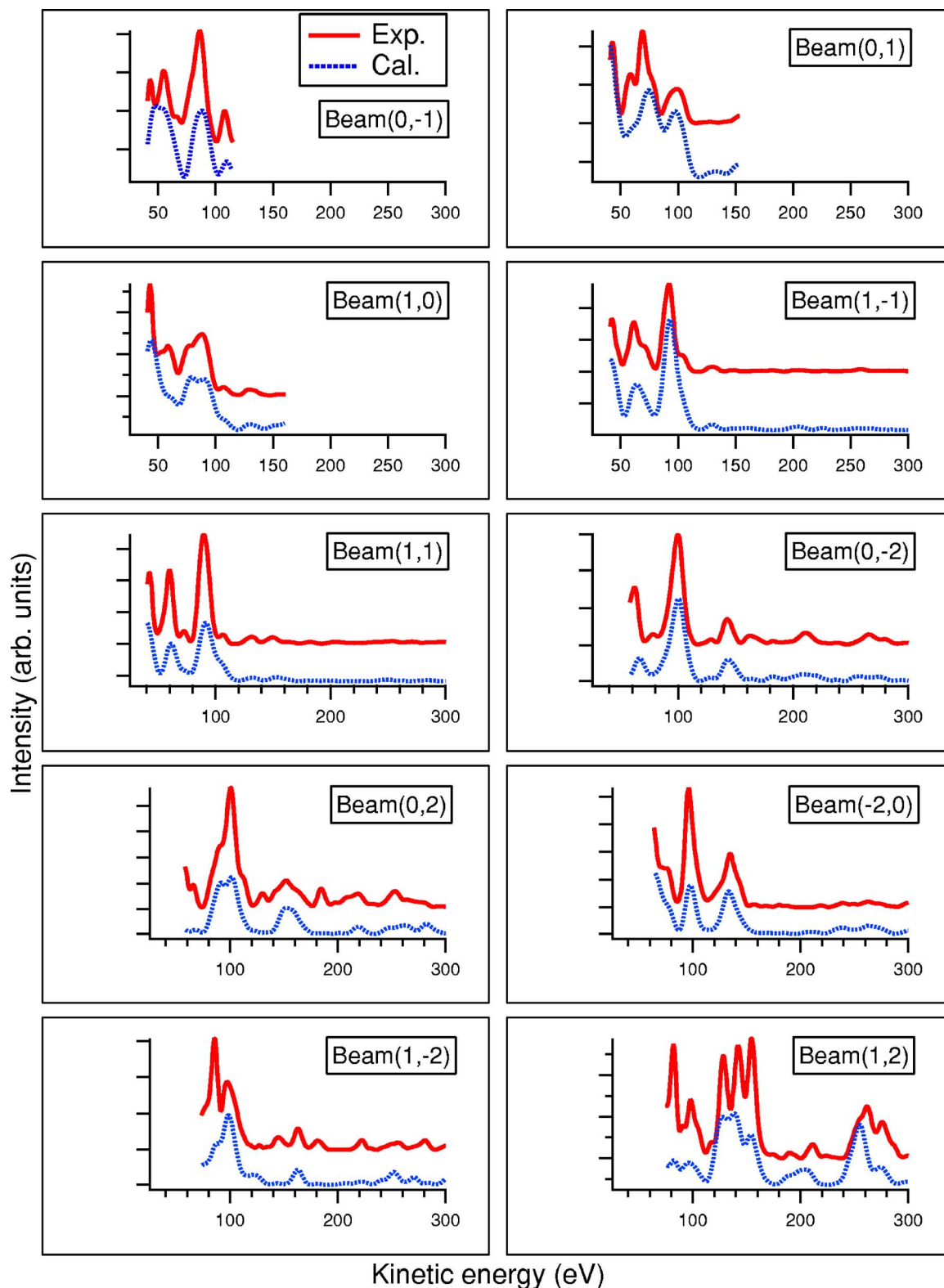


FIG. 3. (Color online) Comparison of 20 experimental and calculated IV curves for normal incidence on Bi(110) at 110 K. Solid lines show experimental data and dotted lines show calculated data which are shifted downward for comparison. To be continued in Fig. 4.

shown in Figs. 3 and 4. 20 symmetry inequivalent beams with a total energy range of 3591 eV have been analyzed to determine the following structural and nonstructural parameters: the first four interlayer spacings d_{ij} ($j=i+1$; $1 \leq i \leq 4$),

the real part of the inner potential V_0 , and Debye temperatures Θ_{D_1} and Θ_{D_2} for atoms in the first and second layers, respectively. The results of the structural analysis are summarized in Table I. Note that the first and the third interlayer

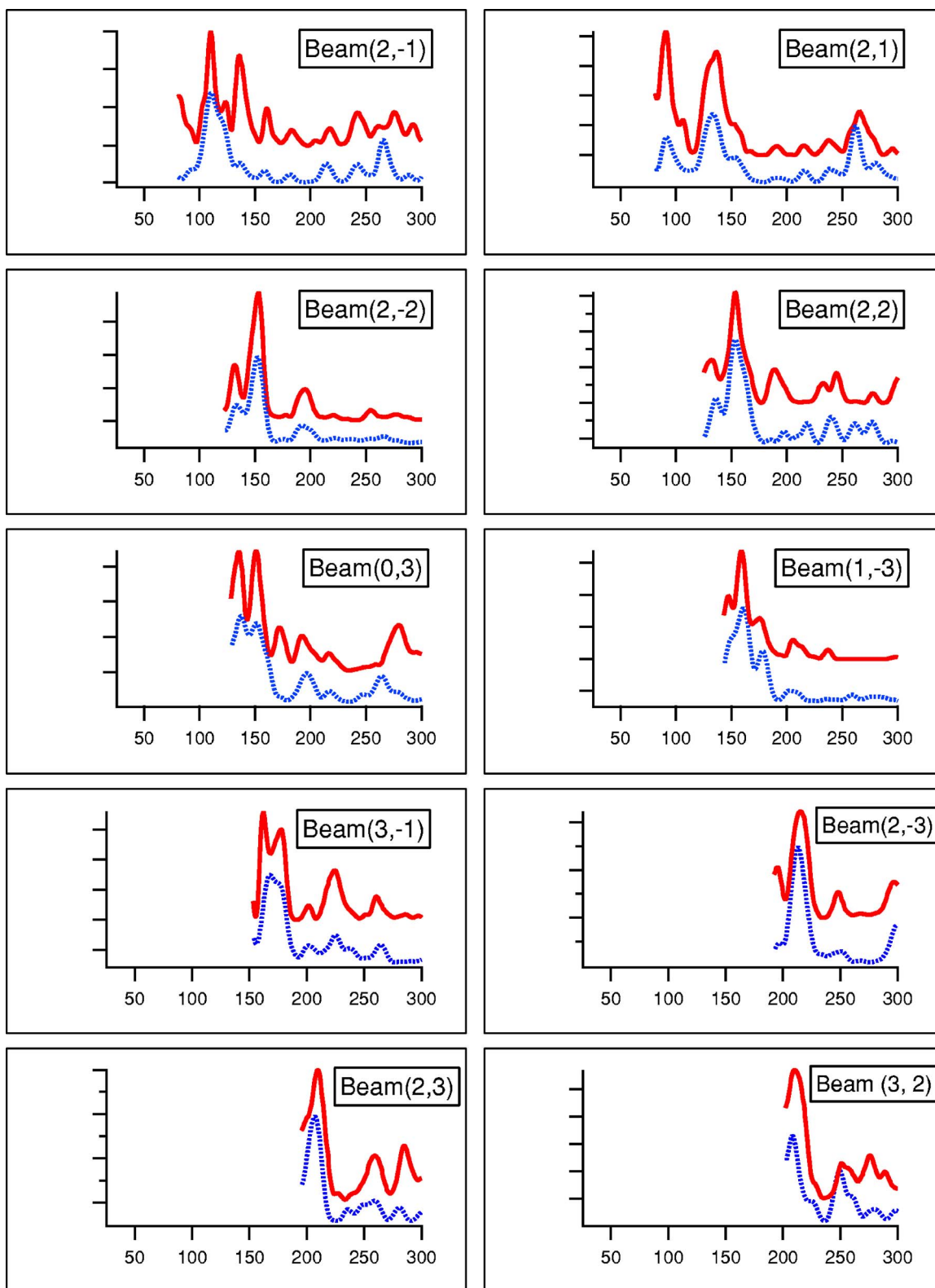


FIG. 4. (Color online) Continuation of Fig. 3.

spacings correspond to the small separation (0.21 \AA) between the two layers making up the bilayer in the bulk. Their seemingly dramatic relative relaxations are very small in absolute terms. Also, the fourth layer appears to move above the third layer by 0.01 \AA . However, this very small value is

clearly below our detection limit. Overall no significant relaxation for the Bi(110) surface is found. We have tried many possible displacement patterns allowed due to the low surface symmetry. However, we found no significant improvement in R_P when changing the relative distance between the

TABLE I. Optimized parameter values for the surface structure of Bi(110) from LEED and *ab initio* calculations. Interlayer spacings between the *i*th and *j*th layers are indicated as d_{ij} . d_{ij}^b is the corresponding interlayer spacing of the truncated bulk at 110 K and $\Delta d_{ij} = d_{ij} - d_{ij}^b$. V_0 is the real part of the inner potential. Θ_{D_1} and Θ_{D_2} are the Debye temperatures for the first and the second layers, respectively.

Parameters	Experimental results by LEED			<i>ab initio</i> calculations
	Starting values	Optimized values	$\Delta d_{ij}/d_{ij}^b$ (%)	$\Delta d_{ij}/d_{ij}^b$ (%)
d_{12} (Å)	0.208	0.18 ± 0.048	-13 ± 23	-62
d_{23} (Å)	3.064	3.06 ± 0.043	-0.2 ± 1.4	+0.3
d_{34} (Å)	0.208	0.01 ± 0.040	-105 ± 19	-105
d_{45} (Å)	3.064	3.20 ± 0.046	$+4.3 \pm 1.5$	+4.4
V_0 (eV)	8.0	3.5 ± 1.50		
Θ_{D_1} (K)	119	95^{+60}_{-25}		
Θ_{D_2} (K)	119	116^{+80}_{-40}		
R_p		0.455		

two basis atoms in the first and second layers parallel to the mirror line. The Debye temperature for the first layer is found to be lower than that of the bulk, which is consistent with an early study of Goodman and Somorjai.²⁴ Reduced surface Debye temperatures are a common phenomenon reflecting the weaker bonding of surface atoms compared to the bulk.²⁵ The actual numerical values of the surface Debye temperature are an important ingredient for the determination of the electron-phonon coupling strength from angle-resolved photoemission data.^{26–29} Meanwhile the second layer shows a Debye temperature close to the bulk value.

The LEED IV analysis gives a relatively high R_p factor of about 0.455 compared to typical values of 0.1 to 0.3 for clean unreconstructed metal surfaces. Many efforts have been made to find out the possible causes. We simulated non-normal-incidence conditions extensively in the LEED IV calculations and found that an increase in the incident angle gave a dramatic rise in the R factor from its minimum at zero or normal incidence. This suggests that the sample is properly aligned and the relatively high value is not caused by deviations from normal incidence during the IV measure-

ment. The influence of the muffin-tin radius on the structure has been studied and results show essentially the same geometry with a minimum R factor at the muffin-tin radius of 2.87 a.u. We also tried the atomic potential derived from our *ab initio* calculations with no significance changes in the optimized structural parameters nor an improvement in the R factor. So it might be the structural complexity and low symmetry of the Bi(110) surface itself that complicates the LEED process. As seen on open semiconductor surfaces, the presence of dangling bonds and the presence of voids in the open surface structure is a real challenge for the muffin-tin approximation of the crystal potential and could also contribute to the relatively high R_p for this surface. However, the low surface symmetry of Bi(110) gives rise to the large number of nonequivalent beams. Here we present an accumulative energy range of 3591 eV (20 beams) which is larger than about 1000 eV used in typical LEED studies. When an overall range of only 1071 eV (the first six beams) was analyzed in our work, the R factor decreased to 0.36 without changes in the optimized structural parameters. This value is comparable to LEED results for many semiconductors and

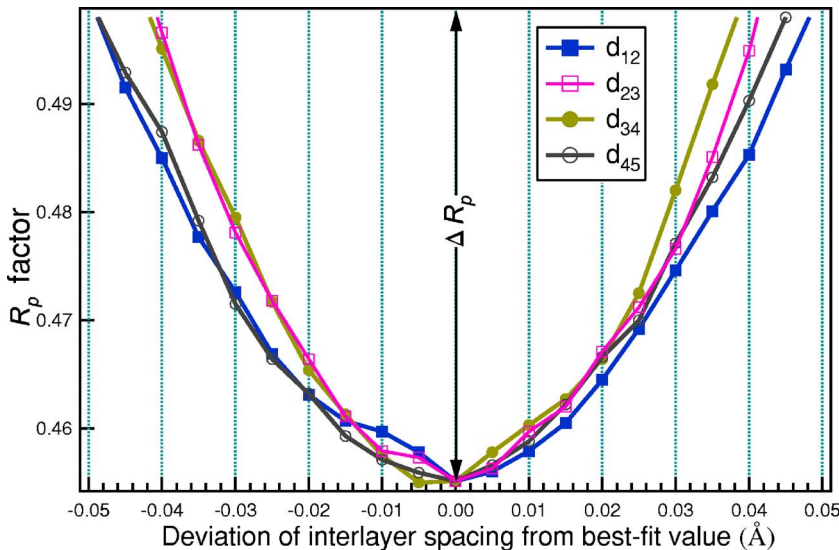


FIG. 5. (Color online) Error bar determination for the first four interlayer spacings based on $\Delta R_p = 0.043$ and Eq. (2).

metal oxide compounds with similar geometric and electronic structures. Interestingly, the reduction of R factor due to fewer beams indicates more intricate scatterings in the higher ordered beams. Furthermore, with horizontal surface atomic displacement in the mirror plane allowed, a smaller R has been obtained but, considering that the displacement values are within error limit and no significant geometry change occurred, we are not including these displacements in the report. The agreement between this large experimental data set and the calculated intensity-energy curves, as shown in Figs. 3 and 4, gives us confidence in the reliability of our results.

The error bars of the optimized parameters were analyzed based on the variation of the R factor around $R_{P \min}$, $\Delta R_P = 0.043$ according to Eq. (2). The dependence of R_P on a change of the interlayer spacings away from their optimized values is shown in Fig. 5. In this analysis, all other parameters were fixed at their optimized values. We can see that all the sensitivity curves take on a parabolic shape. The errors for the individual parameters are also listed in Table I.

B. Comparison to first-principles calculations

The first-principles calculations performed for bulk Bi without the inclusion of spin-orbit interaction give bulk short and long interlayer spacings of 0.142 and 3.087 Å, respectively. Evaluations that include the SOC term lead to a very slight modification of approximately 0.01 Å of these results. As shown in Table I, our scalar relativistic force calculations give the following values for the first four interlayer spacing relaxations at 0 K: $\Delta d_{12}/d_{12}^b = -62\%$, $\Delta d_{23}/d_{23}^b = +0.3\%$, $\Delta d_{34}/d_{34}^b = -105\%$, and $\Delta d_{45}/d_{45}^b = +4.4\%$. These results agree reasonably well with those obtained by the LEED IV analysis at 110 K considering the fact that the absolute distance difference between the experimental and calculated first interlayer relaxations of -13% and -62% is only 0.06 Å. Both the experiment and theory lead to the contraction of the first interlayer spacing. For the second interlayer spacing the theory gives a small expansion while the experiment shows a small contraction of the spacing. However, the theoretical result is within the experimental error bar. The absolute distance difference between the experimental and calculated second interlayer relaxations of 0.015 Å is even

smaller than that for the first interlayer spacing. For the third and fourth interlayer spacings the theory and experiment are in excellent agreement. The first-principles calculations that include the spin-orbit interaction term lead to $\Delta d_{12}/d_{12}^b = -43\%$ and $\Delta d_{23}/d_{23}^b = +0.4\%$ for the first and second interlayer spacings, respectively. These values have been obtained by keeping the interlayer spacings $\Delta d_{34}/d_{34}^b$ and $\Delta d_{45}/d_{45}^b$ equal to those found in the scalar relativistic calculations. This shows that the influence of spin-orbit interaction on the relaxation is small and probably will not change the values of d_{34} and d_{45} significantly. Notice that in the relaxed geometry a change of 6% or 0.01 Å in $\Delta d_{12}/d_{12}^b$ corresponds to an energy change of only 0.5 meV per surface atom, which is certainly at the limit of our accuracy.

In our force calculations, we also optimized the position of the surface atoms in a plane parallel to the surface. By symmetry, this movement is then confined to the mirror plane shown in Fig. 1(a). We notice that these relaxations are small and do not exceed 1.0% in the top four layers, consistent with the experimental findings.

V. CONCLUSIONS

Our results give a consistent picture of the very low-symmetry surface geometric structure of Bi(110) by LEED intensity analysis and first-principles calculations. Good agreement is reached between experimental LEED and theoretical IV curves. No structural reconstruction occurs despite of dangling bonds present at the surface. No significant absolute value of relaxation is found for the first four interlayer spacings. The reduced top-layer Debye temperature suggests essentially larger vibrational atomic amplitudes at the surface. Experimentally, the approach of sample alignment by calculating the diffraction spot positions on the LEED screen is very efficient and can be used for surfaces with low symmetry as well as for *in-situ* cleaved surfaces.

ACKNOWLEDGMENTS

This work was supported by the U.S. National Science Foundation Grant No. DMR-0134933, the Danish National Science Foundation, the Basque Country Government, and the University of the Basque Country.

*Electronic address: jsun@cisunix.unh.edu

†Permanent address: Department of Synchrotron Radiation, Lund University, SE-22100 Lund, Sweden.

¹J.-P. Issi, Aust. J. Phys. **32**, 585 (1979).

²S. Agergaard, C. Søndergaard, H. Li, M. B. Nielsen, S. V. Hoffmann, Z. Li, and P. Hofmann, New J. Phys. **3**, 15.1 (2001).

³P. Hofmann, J. E. Gayone, G. Bihlmayer, Y. M. Koroteev, and E. V. Chulkov, Phys. Rev. B **71**, 195413 (2005).

⁴M. Hengsberger, P. Segovia, M. Garnier, D. Purdie, and Y. Baer, Eur. Phys. J. B **17**, 603 (2000).

⁵C. R. Ast and H. Höchst, Phys. Rev. Lett. **87**, 177602 (2001).

⁶P. Hofmann, Prog. Surf. Sci. **81**, 191 (2006).

⁷Y. M. Koroteev, G. Bihlmayer, J. E. Gayone, E. V. Chulkov, S. Blügel, P. M. Echenique, and P. Hofmann, Phys. Rev. Lett. **93**, 046403 (2004).

⁸J. I. Pascual *et al.*, Phys. Rev. Lett. **93**, 196802 (2004).

⁹F. Jona, H. D. Shih, D. W. Jepsen, and P. M. Marcus, J. Phys. C **12**, L455 (1979).

¹⁰A. B. Shick, J. B. Ketterson, D. L. Novikov, and A. J. Freeman, Phys. Rev. B **60**, 15484 (1999).

¹¹H. Mönig, J. Sun, Y. M. Koroteev, G. Bihlmayer, J. Wells, E. V. Chulkov, K. Pohl, and P. Hofmann, Phys. Rev. B **72**, 085410 (2005).

¹²F. Jona, Surf. Sci. **8**, 57 (1967).

- ¹³M. A. van Hove and S. Y. Tong, *Surface Crystallography by LEED* (Springer-Verlag, Berlin, 1979).
- ¹⁴Y. Liu and R. E. Allen, Phys. Rev. B **52**, 1566 (1995).
- ¹⁵P. Cucka and C. S. Barrett, Acta Crystallogr. **15**, 865 (1962).
- ¹⁶A. Barbieri and M. A. van Hove, <http://www.sitp.lbl.gov/index.php?content=/leedpack/leedpack.html>
- ¹⁷G. Jezequel, A. Barski, P. Steiner, F. Solal, P. Roubin, R. Pinchaux, and Y. Petroff, Phys. Rev. B **30**, 4833 (1984).
- ¹⁸J. B. Pendry, *Low Energy Electron Diffraction* (Academic Press, London, 1974).
- ¹⁹J. B. Pendry, J. Phys. C **13**, 937 (1980).
- ²⁰H. Krakauer, M. Posternak, and A. J. Freeman, Phys. Rev. B **19**, 1706 (1979).
- ²¹E. Wimmer, H. Krakauer, M. Weinert, and A. J. Freeman, Phys. Rev. B **24**, 864 (1981).
- ²²V. L. Moruzzi, J. F. Janak, and A. R. Williams, *Calculated Electronic Properties of Metals* (Pergamon, New York, 1978).
- ²³C. Li, A. J. Freeman, H. J. F. Jansen, and C. L. Fu, Phys. Rev. B **42**, 5433 (1990).
- ²⁴R. M. Goodman and G. A. Somorjai, J. Chem. Phys. **52**, 6325 (1970).
- ²⁵C. Walfried, D. N. McIlroy, J. Zhang, P. A. Dowben, G. A. Katrich, and E. W. Plummer, Surf. Sci. **363**, 296 (1996).
- ²⁶C. R. Ast and H. Höchst, Phys. Rev. B **66**, 125103 (2002).
- ²⁷C. Kirkegaard, T. K. Kim, and P. Hofmann, New J. Phys. **7**, 99 (2005).
- ²⁸J. E. Gayone, C. Kirkegaard, J. W. Wells, S. V. Hoffmann, Z. Li, and P. Hofmann, Appl. Phys. A: Mater. Sci. Process. **80**, 943 (2005).
- ²⁹T. K. Kim, T. S. Sorensen, E. Wolfring, H. Li, E. V. Chulkov, and P. Hofmann, Phys. Rev. B **72**, 075422 (2005).